




Multiparametric High-Resolution MRI as a Tool for Mapping of Hypoxic Level in Tumors

Technology in Cancer Research & Treatment
Volume 17: 1-8
© The Author(s) 2018
Article reuse guidelines:
sagepub.com/journals-permissions
DOI: 10.1177/1533033818797066
journals.sagepub.com/home/tct



Igor Serša, PhD^{1,2}, Franci Bajd, PhD³, Monika Savarin, PhD⁴,
Tanja Jesenko, PhD⁴, Maja Čemažar, PhD⁴, and Gregor Serša, PhD^{4,5}

Abstract

Hypoxia is a condition, common to most malignant tumors, where oxygen tension in the tissue is below the physiological level. Among consequences of tumor hypoxia is also altered cancer cell metabolism that contributes to cancer therapy resistance. Therefore, precise assessment of tumor hypoxia is important for monitoring the tumor treatment progression. In this study, we propose a simple model for prediction of hypoxic level in tumors based on multiparametric magnetic resonance imaging. The study was performed on B16F1 murine melanoma tumors *ex vivo* that were first magnetic resonance scanned and then analyzed for hypoxic level using hypoxia-inducible factor 1- α antibody staining. Each tumor was analyzed in identical sections and in identical regions of interest for pairs of hypoxic level and magnetic resonance values (apparent diffusion coefficient and T_2). This was followed by correlation analysis between hypoxic level and respective magnetic resonance values. A moderate correlation was found between hypoxic level and apparent diffusion coefficient ($\rho = 0.56$, $P < .00001$) and lower between hypoxic level and T_2 ($\rho = 0.38$, $P < .00001$). The data were analyzed further to obtain simple predictive models based on the multiple linear regression analysis of the measured hypoxic level (dependent variable) and apparent diffusion coefficient and T_2 (independent variables). Among the hypoxic level models, the most efficient was the 3-parameter model given by relation ($HL = k_{ADC} ADC + k_{T_2} T_2 + b$), where $k_{ADC} = 26\%/ \mu\text{m}^2/\text{ms}$, $k_{T_2} = 0.8\%/ \text{ms}$, and $b = -32\%$. The model can be used for calculation of the predicted hypoxic level map based on magnetic resonance-measured apparent diffusion coefficient and T_2 maps. Similar prediction models, based on tumor apparent diffusion coefficient and T_2 maps, can be done also for other tumor types *in vivo* and can therefore help in assessment of tumor treatment as well as to better understand the role of hypoxia in cancer progression.

Keywords

multiparametric MRI, tumors, hypoxic level, predictive models, MR microscopy

Abbreviations

ADC, apparent diffusion coefficient; BCNU, 1,3-bis (2-chloroethyl)-1-nitroso-urea; BOLD, blood oxygenation level-dependent; CPMG, Carr-Purcell-Meiboom-Gill; DCE-MRI, dynamic contrast-enhanced magnetic resonance imaging; DWI, diffusion-weighted imaging; HE, hematoxylin and eosin; HL, hypoxic level; IHC, immunohistochemistry; MR, magnetic resonance; MRI, magnetic resonance imaging; OE-MRI, oxygen-enhanced magnetic resonance imaging; PGSE, pulsed-gradient spin-echo; ROI, region of interest.

Received: May 14, 2018; Revised: July 12, 2018; Accepted: July 24, 2018.

¹ Jožef Stefan Institute, Ljubljana, Slovenia

² Institute of Physiology, Medical Faculty, University of Ljubljana, Ljubljana, Slovenia

³ Faculty of Mathematics and Physics, University of Ljubljana, Ljubljana, Slovenia

⁴ Institute of Oncology Ljubljana, Ljubljana, Slovenia

⁵ Faculty of Health Sciences, University of Ljubljana, Ljubljana, Slovenia

Corresponding Authors:

Igor Serša, PhD, Jožef Stefan Institute, Jamova 39, 1000 Ljubljana, Slovenia.

Email: igor.sersa@ijs.si

Gregor Serša, PhD, Institute of Oncology Ljubljana, Zaloška 2, 1000 Ljubljana, Slovenia.

Email: gserša@onko-i.si



Introduction

Tumors mainly consist of highly proliferating cells with high demand on the oxygen supply. In bigger tumors, the oxygen supply often cannot follow its demand due to the unorganized tumor vasculature and the increasing distance between cells and the existing vasculature, which is hampering oxygen diffusion. This creates a low oxygen level that leads to the hypoxic milieu.¹ If oxygenation of a normal tissue is between 4% and 9%, then in the respective tumors it falls down to the range of 1% and 2% or lower.^{2,3} Tumor hypoxia induces different signaling pathways leading to growth of advanced but dysfunctional tumor vascularization, stimulation of a complex cell signaling network in tumor cells, and acquisition of epithelial-to-mesenchymal transition phenotype resulting in cell mobility and metastasis. Furthermore, it also alters cancer cell metabolism and contributes to therapy resistance by inducing cell quiescence.⁴ Therefore, a precise and efficient method of hypoxia measurement in tumors is of high importance for tumor treatment monitoring, and for this task, nuclear magnetic resonance (NMR) and magnetic resonance imaging (MRI) are 2 well-suited methods.^{5,6}

Local oxygen tension in a tissue can be measured by ¹⁹F magnetic resonance spectroscopy. The method utilizes perfluorinated molecular probes, of which the spin-lattice relaxation rate is proportional to the local oxygen tension.^{7,8} This technique was used in preclinical studies, where its efficiency was demonstrated in monitoring changes in oxygen tension⁹ and in phase I clinical studies using nitroimidazole hypoxia markers.¹⁰ However, an important issue remains regarding administration of perfluorinated molecular probes. Intravenous administration is not efficient due to the probe sequestration in the liver and spleen, while their direct administration at the site of measurement is invasive. Overhauser-enhanced MRI is another technique that allows hypoxia imaging by combining MRI with quantitative pO₂ measurements, providing both hypoxia and microvascular permeability data noninvasively.¹¹ Since hypoxic tumors often exhibit poor perfusion, dynamic contrast-enhanced MRI (DCE-MRI) that measures tissue perfusion rates can provide also an insight into the extent of tumor hypoxia. It was found that the DCE-MRI signal increase over baseline correlates with perfusion and therefore also with pO₂.¹² Oxygen-enhanced MRI (OE-MRI) was found also efficient in quantifying tumor hypoxia in preclinical cancer models.¹³ Blood oxygen level-dependent (BOLD) MRI is sensitive to elevated concentrations of endogenous paramagnetic deoxyhemoglobin that result in an increased relaxation rate [$R_2^* = 1/T_2^*$]. As deoxyhemoglobin concentration is closely related to tissue oxygenation, the BOLD signal can be used also as a hypoxia marker.^{14,15} A trend toward a negative correlation was observed between R_2^* and pO₂, suggesting that hypoxic tumors exhibit elevated R_2^* values.¹⁶ Diffusion-weighted imaging (DWI) and apparent diffusion coefficient (ADC) mapping have also been proposed as magnetic resonance (MR) methods that can indirectly assess tumor hypoxia through the hypoxia-associated alterations in

water diffusion.¹⁷⁻¹⁹ Multiparametric MRI utilizes combining some of these methods together, as for example, ADC mapping and DCE-MRI, thus enabling more reliable detection of hypoxic tissue.²⁰

In this study, we present a simple method for prediction of hypoxic level (HL) in tumors, based on multiparametric imaging of tumors including standard mapping techniques, that is, ADC and T_2 mapping. The study was performed on B16F1 murine melanoma tumors that were first MR scanned and then analyzed for HL using hypoxia-inducible factor 1- α (HIF-1 α) antibody staining. Each tumor was analyzed in identical sections and in identical regions of interest (ROIs) for pairs of HL and MR values (ADC and T_2). This was followed by correlation analysis between HL and the respective MR values. Finally, a predictive model for HL based on the multiple regression analysis was proposed.

Materials and Methods

Tumors

Six tumors, selected for the study, were B16F1 murine melanoma. The tumors were induced in female C57Bl/6 mice (Envigo Laboratories, Udine, Italy) with the injection of 10⁶ B16F1 cells (American Type Culture Collection, Manassas, Virginia) in 100 μ L of physiological solution into the shaved right flank of the mice. When the tumors reached 40 or 100 mm³, mice were killed, the tumors were excised and tagged at one end of their long axis with a green tissue marking dye (08-0728-3; Cancer Diagnostics, Inc, Morrisville, North Carolina). Each excised tumor was stored in physiological solution on ice and immediately transported to the MRI facility where the scanning started within next 2 hours after the tumor excision. Before the scanning, the tumors were taken out of solution, gently wiped, and then placed in a 10-mm glass tube with the tagged part up. The tube was then sealed and inserted in the MRI scanner to prevent sample desiccation during the 140-minute MRI scan protocol (Table 1). After the MRI scanning, the tumor samples were fixed in zinc fixative (BD Biosciences, San Diego, California) to make them ready for the immunohistochemical (IHC) staining of hypoxia, as given subsequently.

All animal experiments were conducted in accordance with the guidelines for animal experiments of the European Union Directives and the permission obtained from the Ministry of Agriculture and the Environment of the Republic of Slovenia (Permission No. 34401-3/2012/2), which was given based on the approval of the National Ethics Committee for Experiments on Laboratory Animals.

Magnetic Resonance Imaging of Tumor Samples and Calculation of ADC and T_2

Magnetic resonance microscopy experiments were performed on a high-spatial resolution MR scanner consisting of a 9.4 Tesla (400 MHz proton frequency) vertical bore superconducting magnet (Jastec, Tokyo, Japan) equipped with a

Table 1. Magnetic Resonance Imaging Sequence Parameters.

Sequence Parameter	MRI Sequence		
	3-D Spin-Echo	3-D PGSE DWI	3-D Multiecho
Field of view, mm ³	20 × 10 × 10		
Imaging matrix	128 × 64 × 64	128 × 64 × 16	
Spatial resolution, μm ³	156 × 156 × 156	156 × 156 × 625	
Echo/interecho time, milliseconds	3	32	16
Repetition time, milliseconds	100	1030	1930
Signal averages	1	1	2
Number of echoes	1	1	8
<i>b</i> -values, s/mm ²	/	0, 140, 330, 670	/
Scan time, minutes	7	70	66

Abbreviations: DWI, diffusion-weighted imaging; MRI, magnetic resonance imaging.

Bruker Micro2.5 gradient system (Bruker, Ettlingen, Germany) and by a Tecmag Redstone spectrometer (Tecmag, Houston, Texas). Tumor samples in glass tubes were inserted into a 10-mm-diameter microimaging probe and then scanned by a protocol consisting of the 3-D T_1 -weighted spin-echo imaging sequence for obtaining high-resolution anatomical image of the tumor followed by sequences for ADC and T_2 mapping. The sequences were the 3-D DWI sequence based on the pulsed-gradient spin-echo (PGSE) sequence for ADC mapping and the 3-D multispin-echo imaging sequence based on the Carr-Purcell-Meiboom-Gill (CPMG) multiecho train for T_2 mapping.²¹ The imaging parameters of the applied MR sequences are given in Table 1. During scanning, the samples were kept at a constant temperature of 20°C ± 1°C (Table 1).

The acquired MRI data were analyzed by using in-house written MR image analysis software, developed within the Matlab programming environment (MathWorks, Inc, Natick Massachusetts). In the software, fully automated MR image segmentation was performed as follows. First, for each tumor sample, a 3-D set of DW images with $b = 0$ was used to create a mask for automatic discrimination of the tumor region from the hypointense background as described by Vidmar *et al.*²² The hyperintense regions were considered as the sample regions with the corresponding mask value set to unity, while the hypointense regions were considered as background with the corresponding mask value set to zero. For each tumor sample, the same mask was used to calculate the maps of ADC and of transversal relaxation time T_2 . Specifically, ADC maps were calculated in a pixelwise manner by fitting the Stejskal-Tanner relation,²³ $[I_{DWI}(\vec{r}) = I_{DWI,0}(\vec{r})\exp(-bADC(\vec{r}))]$, to the masked DW images, where $I_{DWI,0}(\vec{r})$ is the signal intensity obtained with pulsed-field gradients equal to zero ($b = 0$), b is the diffusion attenuation factor of the PGSE pulse sequence, and $ADC(\vec{r})$ is the 3-D map of the ADC. T_2 maps were calculated by fitting a monoexponential function,²⁴

$[I_{CPMG}(\vec{r}) = I_{CPMG,0}(\vec{r})\exp(-niTE/T_2(\vec{r}))]$, to the masked CPMG images, where, $I_{CPMG,0}(\vec{r})$ represents the initial signal intensity after the excitation 90° radio frequency (RF) pulse and $n iTE$ (inter echo time) the time point of the n -th echo, while $T_2(\vec{r})$ is the 3-D map of the transversal relaxation time.

Histology of Tumors

The tumor samples were taken from zinc fixative and embedded to paraffin blocks. The blocks were then cut into consecutive sections with thickness of 2 μm through each tumor in orientations that represented best match to the orientations of the acquired MR images (presented in the orientation of the highest in-plane resolution). Orientation matching was enabled by tumor tagging prior to MRI. To estimate the percent of necrosis, every fifth section was stained with hematoxylin and eosin (HE), others were used for IHC staining of hypoxia marker HIF-1α. This study was conducted as a proof of principle and therefore HIF-1α staining was selected due to already optimized staining procedure and good experience from previous studies—the hypoxia level of related B16F10 control tumors was estimated only to 4.7% when stained for HIF-1α.²⁵ The primary antibodies against HIF-1α (ab2185; Abcam, Cambridge, Massachusetts) were applied at dilution 1:500 and then detected with a peroxidase-conjugated streptavidin-biotin system (Rabbit specific horseradish-peroxidase-diaminobenzidine [HRP/DAB] detection IHC kit, ab64261; Abcam) and counterstained with hematoxylin as described previously.²⁵ Each tumor was analyzed in 2 central HIF-1α-stained sections with the best match to the corresponding MR slices. The sections were analyzed in 10 randomly distributed regions per section that uniformly covered all of the tumor's characteristic regions. From the regions, images of 300 × 400 μm² were captured by a BX-51 microscope (Olympus, Hamburg, Germany) under 40× magnification (numerical aperture 0.85) using a DP72 CCD camera (Olympus). Hypoxic regions, that is, HL, was assessed by 3 independent researchers on the acquired images. Only the cells with brown-colored nucleus were considered hypoxic.

Correlation Analysis Between ADC and T_2 Maps and HL

First, in each of the IHC slices, 10 randomly distributed ROIs with a size of 300 × 400 μm² that uniformly covered all characteristic regions of the tumor excluding regions of stroma or tissue with an increased cellularity were selected and average HL values for the selected ROIs were calculated. Then, for each tumor sample, 2 central adjacent MRI slices that corresponded best to the histological slices of the same tumor were selected. Magnetic resonance maps of the selected slices were upscaled to matrix 768 × 384 using bilinear interpolation, and for each of the maps, up to 10 ROIs with the best match to the corresponding ROIs in histological slices were selected, that is, colocalization between ROIs in MR maps and IHC slices was performed. In the MR maps, the selected ROIs corresponded to

regions of 12×16 pixels. In the next step, average ADC and T_2 values from the selected ROIs were calculated. Thus, $N = 94$ measured ADC and T_2 values of the tumors were obtained that were then further analyzed for their correlation with the corresponding HL values using Pearson correlation test.

Predictive Models for HL

Simple predictive models based on the multiple linear regression analysis of the measured HL (dependent variable) and ADC and T_2 (independent variables) data were obtained. The models included both independent variables (3-parameter model) or just ADC (2-parameter model). The regression analysis was performed with the OriginPro program (OriginLab Corporation, Northampton, Massachusetts).

Results

The histological analyses of tumors indicated heterogeneous composition of the studied tumors; predominately there were proliferative cells, some hypoxic and necrotic regions, few fat cells, as well as muscle and connective fibers. Such composition can be seen in Figure 1A that shows a histological (HE stained) image of a central slice across a representative B16F1 murine melanoma tumor. The image in Figure 1B from the neighboring slice of the same tumor is HIF-1 α antibody stained to enable determination of HL for each of the selected ROIs. However, the determination is possible when the image is inspected under $40\times$ magnification so that the structure of individual cells can be clearly seen. Images in Figure 1C correspond to 3 different characteristic regions of the tumor analyzed by ROIs with the size of $300 \times 400 \mu\text{m}^2$ in identical positions in HE-stained (right) and HIF-1 α -stained (left) images. The regions correspond to a viable tumor part (region 1), connective tissue (region 2), and necrosis (region 3). Viable tumor cells have intact cell nuclei that color in blue in the HIF-1 α -stained images, while cell nuclei of hypoxic tumor cells color in brown in the same image. This is because the nuclei of hypoxic cells are altered by having present the transcription factor HIF-1 α . The corresponding proportions of the altered cells against all cells in ROI were considered as HLs (Figure 1).

Corresponding tumor slices, which were analyzed by IHC for determination of HL, were firstly scanned by MRI with a protocol consisting of T_1 -weighted imaging and ADC and T_2 mapping. Figure 2 shows an example of the images obtained for the same tumor and slice as shown in Figure 1. The T_1 -weighted image in Figure 2A indicates tumor anatomy; however, it does not offer much information on its structural and functional properties. For providing these, MR maps are much more appropriate. The highest sensitivity to structural changes associated with hypoxia can be seen in the ADC map (Figure 2B), which has relatively uniform low ADC background with values less than $0.8 \mu\text{m}^2/\text{ms}$. In the hypoxic region, it can increase substantially and can go up to $2 \mu\text{m}^2/\text{ms}$, which is almost ADC of bulk water. Differences among grades of

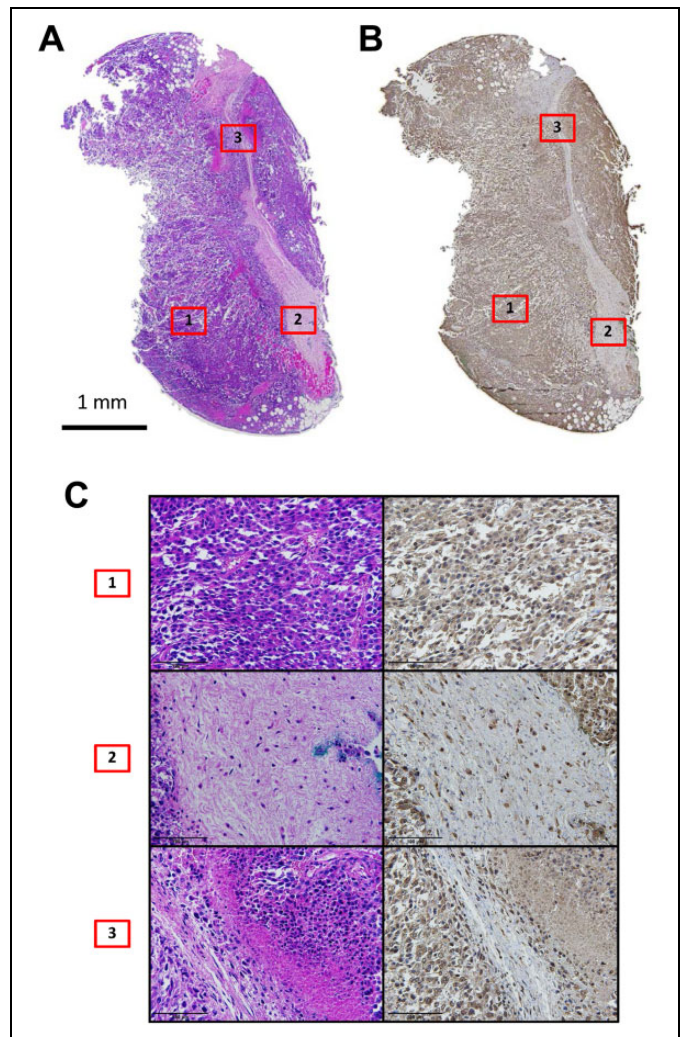


Figure 1. A histologically analyzed B16F1 murine melanoma tumors. Hematoxylin and eosin staining (A) and IHC detection of HIF-1 α marker (B) indicated on a several tumor parts. Scale bar = 1 mm. Different tumor parts (C) were further analyzed under $40\times$ magnification (scale bar = $100 \mu\text{m}$) with HE (C, left) and hypoxia-inducable factor 1-alpha (C, right). The tumor sections represented viable tumor part (1), connective tissue (2), and necrosis (3). The positive hypoxic cells have brown-colored nucleus. HE indicates hematoxylin and eosin; IHC, immunohistochemistry.

tissue hypoxia are less pronounced in the T_2 map (Figure 2C), where the increase of T_2 values in the hypoxic region in comparison to the nonhypoxic tissue background is close to 50%, that is, from approximately 40 milliseconds to up to 60 milliseconds or even more (Figure 2).

Correlations between the measured HL values and the corresponding ADC and T_2 values, as obtained from the selected ROIs of all the tumors, are shown in the graphs in Figure 3. It can be seen that the correlation is higher between HL and ADC (Person correlation coefficient; $\rho = 0.56$, $P < .00001$) than between HL and T_2 ($\rho = 0.38$, $P < .00001$). Dashed lines in the graphs in Figure 3 correspond to trend lines obtained by linear regression, which are given by equations: $\text{ADC} = 0.010$

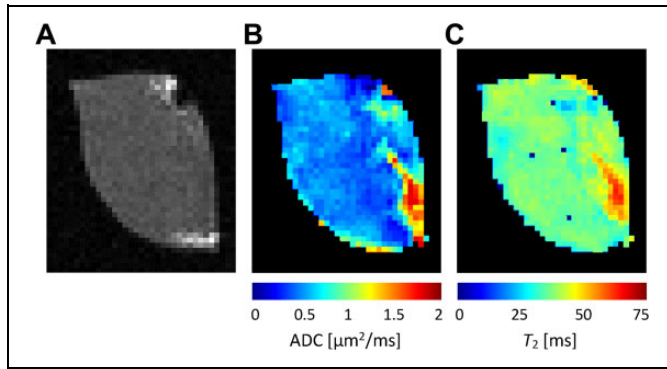


Figure 2. T_1 -weighted image (A) and MR maps of ADC (B) and T_2 (C) values of the same tumor and slice as shown in Figure 1. Among all maps, the ADC map exhibited the largest variability of its values that well correlate with hypoxia; high ADC values were found in the region that coincides with the hypoxic region in Figure 1. Less pronounced correlation with hypoxia was observed for T_2 values. ADC indicates apparent diffusion coefficient; MR, magnetic resonance.

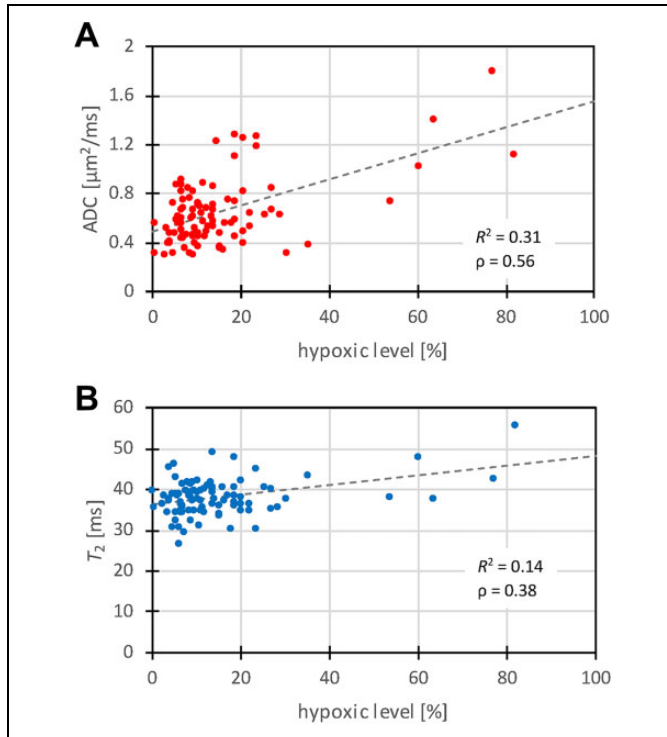


Figure 3. Graphs of correlation between hypoxic level and the corresponding ADC (a) and T_2 (b) values as measured from the selected ROIs for all tumors ($N = 94$). The correlation is higher between HL and ADC than between HL and T_2 . Dashed lines in the graphs correspond to trend lines. ADC indicates apparent diffusion coefficient; HL, hypoxic level; ROI, region of interest.

$\mu\text{m}^2/\text{ms}/\% \text{ HL} + 0.50 \mu\text{m}^2/\text{ms}$ (coefficient of determination $R^2 = 0.31$) and $T_2 = 0.12 \text{ ms}/\% \text{ HL} + 36 \mu\text{m}^2/\text{ms}$ ($R^2 = 0.14$). From the graphs it can also be seen that most measured data points (pairs of HL and the corresponding values of ADC and T_2) were obtained with low HL values and fewer with high

Table 2. Best Fit Model Parameters.

Model	k_{ADC} , $\%/\mu\text{m}^2/\text{ms}$	k_{T_2} , $\%/\text{ms}$	b , $\%$	R^2	ΔHL
3 Parameter ^a	26.0 ± 4.6	0.77 ± 0.28	-31.7 ± 10.4	0.36	11.7
2 Parameter ^b	29.6 ± 4.6		-4.6 ± 3.3	0.31	12.1

Abbreviations: ADC, apparent diffusion coefficient; HL, hypoxic level.

^aThree-parameter model $\text{HL} = k_{\text{ADC}} \text{ADC} + k_{T_2} T_2 + b$.

^bTwo-parameter model $\text{HL} = k_{\text{ADC}} \text{ADC} + b$.

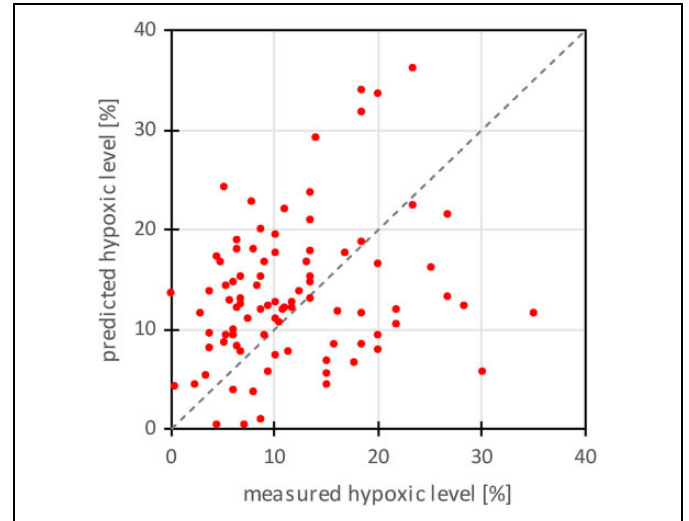


Figure 4. A graph of correlation between the measured hypoxic level (HL) and the predicted HL using the 3-parameter model that required measurement of ADC and T_2 maps. Dashed line in the graph represents a line of ideal correlation ($\rho = 1$). ADC indicates apparent diffusion coefficient.

HL values. This can be explained by a domination of tumors of smaller volumes that were still well oxygenized at the excision time (Figure 3).

Two different multiple linear regression models for HL prediction were fitted to the data: 3-parameter model with independent variables ADC and T_2 and 2-parameter model with the independent variable ADC. The best fit model parameters are shown in Table 2. From the table it can be seen that the 3-parameter model has a better quality of the fit ($R^2 = 0.36$) than the 2-parameter model ($R^2 = 0.31$). The graph in Figure 4 depicts correlation between the measured HL and the predicted HL with the 3-parameter model. The error of the prediction is $\Delta\text{HL} = 11.7\%$, while the correlation coefficient between the measured and the predicted HL values is equal to $\rho = 0.60$, $P < .00001$. The dashed line in the graph represents a line of the ideal correlation ($\rho = 1$; Figure 4).

Figure 5 depicts a map of predicted HL for the tumor and slice from Figure 2. The map was calculated from the corresponding ADC and T_2 maps by using the 3-parameter model for HL prediction (Table 2). Comparison of the map with the ADC and T_2 map shows identical region of an increased signal, however with a much responsive function to changes of ADC and T_2 .

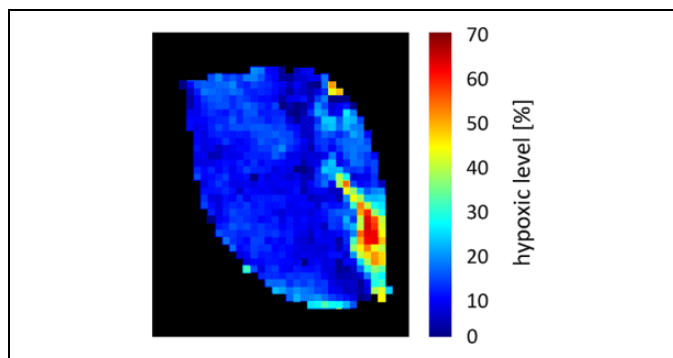


Figure 5. A predicted map of HL as obtained from ADC and T_2 maps by using the 3-parameter model for the same tumor and slice as shown in Figure 2. ADC indicates apparent diffusion coefficient.

In the HL map, there is a bigger difference between the signal in the hypoxic region and the nonhypoxic background than in the corresponding ADC and T_2 maps (Table 2; Figure 5).

Discussion

The aim of our study was to find a possible correlation between immunohistochemically determined HL in tumors and standard MR maps (ADC and T_2). This study was motivated by the studies where ADC mapping was found as an efficient marker for the integrity of tumor cellularity^{17,18}; however, a correlation between HL and ADC or other standard MR maps was not analyzed. The study was performed on murine melanoma tumors B16F1 of different sizes that were not subjected to any therapy. These tumors are highly proliferative and they were excised when their volumes were still small (up to 100 mm³) and were therefore still well oxygenated. Due to this fact, the level of hypoxia was in average low, especially in the viable tumor parts. Therefore, the study could be expanded to larger tumors with more hypoxia in the future. The higher percentage of hypoxic cells was detected in necrotic cells, prior to cell death. High predicted values for the HL were found also in nontumor connective tissues; however, these values could be inaccurate as predictive model parameters were calculated by excluding these tissues from the analysis. In the remaining tissues, the measured HL values are in accordance with different cell density and tissue structure across the tumor.

The study was performed *ex vivo*, that is, tumors were excised, MR scanned, and then histologically analyzed. During the analysis, the tumor tissue oxygenation was low. Therefore, the methods that can measure only current tissue oxygenation would give irrelevant results for hypoxia in live tumors. For that reason, the study was focused on the reliable and permanent markers for hypoxia. Such is the transcriptional factor for HIF-1 α , which can be detected accurately after proper tissue excision and storage. HIF-1 α is a tumor hypoxia marker and it's a key regulator of cellular and developmental response.²⁶ Although other markers are also used for assessing hypoxic regions, such as CAIX, GLUT-1, MCT1, or pimonidazole, neither of them strongly and consistently correlates with

hypoxia, but were demonstrated to colocalize in tumor sections.²⁷ Therefore, a combination of these markers could better predict hypoxic regions, also due to the fact that HIF-1 can also be upregulated under other stimulants.²⁸ Adequate markers for physiological conditions of tumors before their excision are also MRI-measurable values of ADC and T_2 . Apparent diffusion coefficient is sensitive to the internal structure of the tumor in relation to the mobility of water molecules. Its value is high when the ratio between extracellular and intracellular fluid is high, so that there is a lot of free space for water molecules to diffuse freely. On the other hand, its value is low when cells are compacted, which presents restrictions for diffusive motion of water molecules. Relaxation time T_2 is sensitive to the micro-environment of the water molecules, which can be in tumor tissue considered as a porous structure. Molecules close to the surface experience an increased T_2 relaxation, due to the surface relaxation strength posed by paramagnetic centers in the cell walls, while molecules further away have T_2 relaxation of the bulk fluid.²⁹ Because of the effect, a tissue with compacted cells, where surface to volume ratio is high, has shorter T_2 value than the tissue with loosened cells where surface to volume ratio is lower. This effect also explains why ADC and T_2 values are in a positive correlation (which can be deduced from their positive correlation with HE in Figure 3A and B).

Results of our study are in accordance with results of a study by Moffat *et al* where functional diffusion maps were proposed as a biomarker for the early prediction of cancer treatment outcome.¹⁸ It was found that in the vast part of the brain tumors treated with BCNU 9L, ADC values increased over the baseline and that the increase was dose proportional. The ADC increase was explained by the increase of the fractional volume of the interstitial space due to loss of cell membrane integrity and subsequent loss in overall cellular density. In our study, such tissue conditions are associated also with an increased HL and from there stems a positive correlation between HL and ADC, as well as between HL and T_2 . However, such interpretation requires carefulness. In the same study, an opposite response to the treatment was found where ADC decreased due to the decrease in the interstitial fractional volume. This was found in some isolated tumor regions receiving lower drug doses. If HL was also increased in the tissue, then the trend for this part of the tissue would be the opposite (negative correlation between HL and ADC as well as between HL and T_2). As noted, such conditions could be expected at lower treatment doses, that is, lower ADC and HL changes. This could also explain large scattering of points at the origin of the HL and ADC, and HL and T_2 correlation plots (Figure 3A and B).

The study was not performed *in vivo*; therefore, ADC and T_2 values of the excised tumors differ from the corresponding values that would be obtained *in vivo*. In a study by Fan *et al*, it is shown that there exists a strong correlation between *in vivo* and *ex vivo* for ADC and T_2 values of invasive tumors and that ADC values *in vivo* are higher than the corresponding ADC values *ex vivo* (mainly due to a slower diffusion at room temperature than at body temperature), while T_2 values of the

tumors *in vivo* and *ex vivo* stay about the same.³⁰ Salinity of the suspension in which tumors were stored during MRI scanning could also influence the measured ADC based on the osmotic processes that result in the change of the ratio between intra- and extracellular water. Another limitation of the study is also a relatively low number of the analyzed sample points (94 points in 6 different tumors) with its associated use of the same data set for model development and its validation. Another possible source of error in the ROI-based measurement as opposed to the volumetric approach is bias introduced by difficulties in finding optimal match between ROIs selected in MRI and histological images. A disadvantage of the study design is also in inability of measuring tumor tissue oxygenation by other already established MRI methods, such as OE-MRI or DCE-MRI.^{12,13} However, the *ex vivo* study design has also advantages. One is that the tumors were scanned longer and therefore at a higher spatial resolution. This in return enabled comparative examination of the tumors by ADC or T_2 MR mapping and HIF-1 α histology in multiple points per sample; in the study, each tumor was examined in up to 20 points corresponding to different tumor characteristic structures. In most similar studies done *in vivo*, the examined tumors were studied as a whole, that is, each tumor in just 1 point representing its average properties.¹⁹

This *ex vivo* study can serve as a proof of concept that ADC and T_2 maps of tumors can be used as markers for tumor hypoxia. Similar ADC- and T_2 -based prediction models for tumor hypoxia to these presented in this study can be done also for other tumors *in vivo*. In addition, ADC and T_2 mapping sequences are standard of care and are available on most clinical MRI scanners, which makes the prediction models easily transferable to clinical environment. Accurate prediction models can be of significant clinical relevance as they can be used to evaluate therapeutic outcomes. In cancer research, they are important also as a tool for studying the role of hypoxia in cancer treatment or they could have impact on studying other medical phenomena as well.

Conclusion

A simple, yet efficient 3-parameter linear prediction model for prognosis of HL in tumors is presented. Input parameters for the model are ADC and T_2 maps that were found relevant for the prognosis. Based on the model, a map of HL can be calculated. The presented approach can be translated to other tumors *in vivo* so that the corresponding models could help in assessment of tumor treatment and to better understand the role of hypoxia in cancer progression.

Acknowledgments

The authors thank Ana Sepe for providing technical assistance for the study.


Declaration of Conflicting Interests


The author(s) declared no potential conflicts of interest with respect to the research, authorship, and/or publication of this article.


Funding

The author(s) disclosed receipt of the following financial support for the research, authorship, and/or publication of this article: This work was supported by the Slovenian Research Agency grant P3-0003 (Development and evaluation of new approaches to cancer treatment).

ORCID iD

Monika Savarin, PhD  <http://orcid.org/0000-0002-8316-8110>

Maja Čemažar, PhD  <http://orcid.org/0000-0002-1418-1928>

Gregor Serša, PhD  <http://orcid.org/0000-0002-7641-5670>

References

1. Semenza GL. Hypoxia, clonal selection, and the role of HIF-1 in tumor progression. *Crit Rev Biochem Mol.* 2000;35(2):71-103.
2. Muller M, Padberg W, Schindler E, et al. Renocortical tissue oxygen pressure measurements in patients undergoing living donor kidney transplantation. *Anesth Analg.* 1998;87(2):474-476.
3. Dings J, Meixensberger J, Jager A, Roosen K. Clinical experience with 118 brain tissue oxygen partial pressure catheter probes. *Neurosurgery.* 1998;43(5):1082-1094.
4. Muz B, de la Puente P, Azab F, Azab AK. The role of hypoxia in cancer progression, angiogenesis, metastasis, and resistance to therapy. *Hypoxia.* 2015;3:83-92.
5. Pacheco-Torres J, Lopez-Larrubia P, Ballesteros P, Cerdan S. Imaging tumor hypoxia by magnetic resonance methods. *NMR Biomed.* 2011;24(1):1-16.
6. Walsh JC, Lebedev A, Aten E, Madsen K, Marciano L, Kolb HC. The clinical importance of assessing tumor hypoxia: relationship of tumor hypoxia to prognosis and therapeutic opportunities. *Antioxid Redox Signal.* 2014;21(10):1516-1554.
7. Clark LC, Jr, Ackerman JL, Thomas SR, et al. Perfluorinated organic liquids and emulsions as biocompatible NMR imaging agents for ¹⁹F and dissolved oxygen. *Adv Exp Med Biol.* 1984; 180:835-845.
8. Parhami P, Fung BM. F-19 relaxation study of perfluoro chemicals as oxygen carriers. *J Phys Chem.* 1983;87(11):1928-1931.
9. Bourke VA, Zhao D, Gilio J, et al. Correlation of radiation response with tumor oxygenation in the Dunning prostate R3327-AT1 tumor. *Int J Radiat Oncol Biol Phys.* 2007;67(4): 1179-1186.
10. Lee CP, Payne GS, Oregoni A, et al. A phase I study of the nitroimidazole hypoxia marker SR4554 using ¹⁹F magnetic resonance spectroscopy. *Br J Cancer.* 2009;101(11):1860-1868.
11. Matsumoto S, Yasui H, Batra S, et al. Simultaneous imaging of tumor oxygenation and microvascular permeability using overhauser enhanced MRI. *Proc Natl Acad Sci U S A.* 2009;106(42): 17898-17903.
12. Lancaster JA, Carrington BM, Sykes JR, et al. Prediction of radiotherapy outcome using dynamic contrast enhanced MRI of carcinoma of the cervix. *Int J Radiat Oncol.* 2002;54(3):759-767.
13. O'Connor JPB, Boulton JKR, Jamin Y, et al. Oxygen-enhanced MRI accurately identifies, quantifies, and maps tumor hypoxia in pre-clinical cancer models. *Cancer Res.* 2016;76(4):787-795.
14. Taylor NJ, Baddeley H, Goodchild KA, et al. BOLD MRI of human tumor oxygenation during carbogen breathing. *J Magn Reson Imaging.* 2001;14(2):156-163.

15. Zhao D, Pacheco-Torres J, Hallac RR, et al. Dynamic oxygen challenge evaluated by NMR T1 and T2*—insights into tumor oxygenation. *NMR Biomed.* 2015;28(8):937-947.
16. Chopra S, Foltz WD, Milosevic MF, et al. Comparing oxygen-sensitive MRI (BOLD R2*) with oxygen electrode measurements: a pilot study in men with prostate cancer. *Int J Radiat Biol.* 2009;85(9):805-813.
17. Ross BD, Moffat BA, Lawrence TS, et al. Evaluation of cancer therapy using diffusion magnetic resonance imaging. *Mol Cancer Ther.* 2003;2(6):581-587.
18. Moffat BA, Chenevert TL, Meyer CR, et al. The functional diffusion map: an imaging biomarker for the early prediction of cancer treatment outcome. *Neoplasia.* 2006;8(4):259-267.
19. Hompland T, Ellingsen C, Galappathi K, Rofstad EK. DW-MRI in assessment of the hypoxic fraction, interstitial fluid pressure, and metastatic propensity of melanoma xenografts. *BMC Cancer.* 2014;14:92.
20. Lemasson B, Bouchet A, Maisin C, et al. Multiparametric MRI as an early biomarker of individual therapy effects during concomitant treatment of brain tumours. *NMR Biomed.* 2015;28(9):1163-1173.
21. Foucat L, Benderbous S, Bielicki G, Zanca M, Renou JP. Effect of brine injection on water dynamics in postmortem muscle—study of T-2 and diffusion-coefficients by MR microscopy. *Magn Reson Imaging.* 1995;13(2):259-267.
22. Vidmar J, Kralj E, Bajd F, Sersa I. Multiparametric MRI in characterizing venous thrombi and pulmonary thromboemboli acquired from patients with pulmonary embolism. *J Magn Reson Imaging.* 2015;42(2):354-361.
23. Kuchel PW, Pages G, Nagashima K, et al. Stejskal-tanner equation derived in full. *Concept Magn Reson A.* 2012;40a(5):205-214.
24. Gossuin Y, Hocq A, Gillis P, Vuong QL. Physics of magnetic resonance imaging: from spin to pixel. *J Phys D Appl Phys.* 2010;43:213001.
25. Savarin M, Kamensek U, Cemazar M, Heller R, Sersa G. Electrotransfer of plasmid DNA radiosensitizes B16F10 tumors through activation of immune response. *Radiol Oncol.* 2017;51(1):30-39.
26. Iyer NV, Kotch LE, Agani F, et al. Cellular and developmental control of O2 homeostasis by hypoxia-inducible factor 1 alpha. *Genes Dev.* 1998;12(2):149-162.
27. Rademakers SE, Lok J, van der Kogel AJ, Bussink J, Kaanders JHAM. Metabolic markers in relation to hypoxia; staining patterns and colocalization of pimonidazole, HIF-1 alpha, CAIX, LDH-5, GLUT-1, MCT1 and MCT4. *BMC Cancer.* 2011;11:167.
28. Bilton RL, Booker GW. The subtle side to hypoxia inducible factor (HIFalpha) regulation. *Eur J Biochem.* 2003;270(5):791-798.
29. Brownstein KR, Tarr CE. Spin-lattice relaxation in a system governed by diffusion. *J Magn Reson.* 1977;26(1):17-24.
30. Fan XB, Macleod K, Mustafi D, et al. Correlation of in vivo and ex vivo ADC and T2 of in situ and invasive murine mammary cancers. *Plos One.* 2015;10(7):e0129212.